C. R. Physique 11 (2010) 192–203

Contents lists available at ScienceDirect

Comptes Rendus Physique

www.sciencedirect.com

Multiscale NMR and relaxation / RMN et relaxation multi-échelles

Multi-scales nuclear spin relaxation of liquids in porous media

Relaxation magnétique nucléaire multi-échelles des liquides dans les milieux poreux

Jean-Pierre Korb

Physique de la matière condensée, École polytechnique, CNRS, 91128 Palaiseau, France

ARTICLE INFO

Article history:
Available online 16 August 2010

Keywords:
Nuclear spin relaxation
Fast field-cycling relaxation
Two-dimensional spin correlation T_1–T_2
Porous media
Cement pastes
Rocks

Mots-clés :
Relaxation magnétique nucléaire
Relaxation en champ magnétique variable
Corrélation de spin à deux dimensions T_1–T_2
Milieux poreux
Pâtes de ciment
Roches

ABSTRACT

The magnetic field dependence of the nuclear spin–lattice relaxation rate $1/T_1(\omega_0)$ is a rich source of dynamical information for characterizing the molecular dynamics of liquids in confined environments. Varying the magnetic field changes the Larmor frequency ω_0, and thus the fluctuations to which the nuclear spin relaxation is sensitive. Moreover, this method permits a more complete characterization of the dynamics than the usual measurements as a function of temperature at fixed magnetic field strength, because many common solvent liquids have phase transitions that may alter significantly the character of the dynamics over the temperature range usually studied. Further, the magnetic field dependence of the spin–lattice relaxation rate, $1/T_1(\omega_0)$, provides a good test of the theories that relate the measurement to the microdynamical behavior of the liquid. This is especially true in spatially confined systems where the effects of reduced dimensionality may force more frequent reencounters of the studied proton spin-bearing molecules with paramagnetic impurities at the pore surfaces that may alter the correlation functions that enter the relaxation equations in a fundamental way. We show by low field NMR relaxation that changing the amount of surface paramagnetic impurities leads to striking different pore-size dependences of the relaxation times T_1 and T_2 of liquids in pores.
Here, we focus mainly on high surface area porous materials including calibrated porous silica glasses, granular packings, heterogeneous catalytic materials, cement-based materials and natural porous materials such as clay minerals and rocks. Recent highlights NMR relaxation works are reviewed for these porous materials, like continuous characterization of the evolving microstructure of various cementitious materials and measurement of wettability in reservoir carbonate rocks. Although, the recent applications of 2-dimensional T_1–T_2 and T_2-z-store-T_2 correlation experiments for characterization of water exchange in connected micropores of cement pastes are also outlined.
© 2010 Académie des sciences. Published by Elsevier Masson SAS. All rights reserved.

RÉSUMÉ

Les variations des vitesses de relaxation spin-réseau $1/T_1(\omega_0)$ avec le champ magnétique permettent d'obtenir des informations précises sur la dynamique des liquides dans les milieux confinés. Varier le champ magnétique permet de varier les fréquences de Larmor ω_0 sur quatre ordres de grandeur et donc d'élargir considérablement le domaine spectral des fluctuations ressenties par les processus de relaxation magnétique nucléaire. Cette méthode est préférable à la méthode traditionnelle de caractérisation de la dynamique des liquides par la variation de $1/T_1$ avec la température à champ magnétique constant car beaucoup de liquides ont des transitions de phase qui viennent perturber la dynamique mesurée dans la gamme de température utilisée. De plus, l'analyse théorique des profils

E-mail address: jean-pierre.korb@polytechnique.fr.

1631-0705/$ – see front matter © 2010 Académie des sciences. Published by Elsevier Masson SAS. All rights reserved.
doi:10.1016/j.crhy.2010.06.015

de dispersion $1/T_1(\omega_0)$ permet de tester efficacement les théories de relaxation utilisées. Ceci est particulièrement vrai dans le cas des liquides confinés dans les milieux poreux où les effets de dimensionnalité réduite amplifient les occurrences des collisions avec les impuretés paramagnétiques présentes à la surface des pores. Il en résultera des modifications drastiques du comportement des fonctions de corrélation aux temps longs et donc des densités spectrales qui en résultent à basses fréquences. La modification de la quantité d'impuretés paramagnétiques aux interfaces liquide–solide et la variation avec la taille des pores des temps de relaxation de spin T_1 et T_2 nous a permis de connaître le processus de relaxation limitant dans les milieux poreux.
On s'intéressera plus particulièrement aux matériaux poreux à grande surface spécifique comme les verres poreux calibrés de silice, les empilements granulaires compacts, les matériaux catalytiques hétérogènes, les matériaux cimentaires et les matériaux minéraux poreux naturels comme les argiles et les roches. On présentera succinctement nos résultats de relaxation récents sur le suivi en continu de l'évolution de la microstructure des pâtes de ciment et des bétons de poudres réactives et sur la mesure de la mouillabilité des carbonates de réservoir pétrolier. Enfin, nous aborderons brièvement le domaine prometteur des applications récentes des spectres de corrélation à deux dimensions, à bas champ magnétique constant, des temps de relaxation T_1–T_2 and T_2-z-store-T_2 qui ont permis de caractériser un échange d'eau entre les micropores connexes des pâtes de ciment.

© 2010 Académie des sciences. Published by Elsevier Masson SAS. All rights reserved.

1. Introduction

How is it possible to obtain structural and dynamical information on liquids at a pore surface by nuclear spin-relaxation methods? The question is central to understanding texture and transport properties in high surface-area microporous materials, chromatographic supports, heterogeneous catalytic materials, cement and natural macroporous materials such as clays, minerals or porous rocks. The question is also relevant for NMR well-logging, which is now routinely used to determine the fundamental properties of reservoir rocks, such as porosity, pore size distribution, wettability and saturation. However, probing directly the molecular surface dynamics by standard nuclear relaxation methods is difficult. For instance, the very low fraction of molecules in a surface layer in fast exchange with the local bulk phase prevents any direct measurement of the surface molecular dynamics. Several attempts have been proposed to probe surface molecular behavior by standard techniques [1–6]. However, the proposed methods require progressive liquid saturation that is difficult to control. The spin–spin and spin–lattice relaxation rate measurements for a series of saturated calibrated microporous silica glasses, with or without surface silanization, has allowed separation of the surface and bulk contributions [3–5], thus leading to information on the surface reorientational dynamics [6]. Non-standard nuclear magnetic relaxation dispersion experiments (NMRD) [7,8] were also proposed [9,10]. For instance, these methods have shown striking differences between water and aprotic liquids in contact with microporous glass surfaces containing trace paramagnetic impurities [11,12]. All these experimental attempts were concerned with high surface-area materials. Recently, we have proposed to extend their domain of application to macroporous systems with low surface to volume ratio, such as granular packings [13,14] and oil-bearing rocks [15]. NMRD were also concerned with probing directly the dynamics of proton species at the pore surfaces and specific surface areas of cement-based materials [16]. Similar methods gave information about the microstructure time-evolution of hydrated cement pastes [17,18]. More recently, low field two-dimensional NMR relaxation studies: T_1–T_2 [19] and T_2–T_2 [20] evidence exchange of water between the connected micropores of white cement. The method has been also applied to evidence water exchange in porous rock [21], smectite gel with clay [22] and water and oil in rocks [23]. Other low-field two-dimensional NMR experiments correlating diffusion coefficient D and T_2 relaxation time were particularly useful for separating oil and water downhole in petroleum wells [24].

We discuss here the role of low field NMR relaxometry at fixed magnetic field and nuclear magnetic relaxation dispersion (NMRD) experiments for probing physical and chemical properties of various liquids in confinement. We present different applications of these multi-scales nuclear spin relaxation methods on microporous silica glasses, granular packings, cement-based materials and macroporous rocks.

2. Nuclear spin relaxation of liquids within pores

2.1. What is the limiting relaxation process in pores?

Basically, there are two limiting cases in the theoretical description of the relaxation of liquids filling pores with surface relaxation sinks [25]. These cases are either slow-diffusion or fast-diffusion (surface-limited) relaxation, providing that bulk diffusion or surface processes dominate, respectively. Theoretical expressions of the nuclear relaxation rates have been proposed in each limited case [25]. In particular, special interest has been focused on the fast-diffusion relaxation, corresponding to most of the natural rock data (Fig. 1a). In order to discuss the pore-size relaxation data presented in Figs. 1b, 1c,

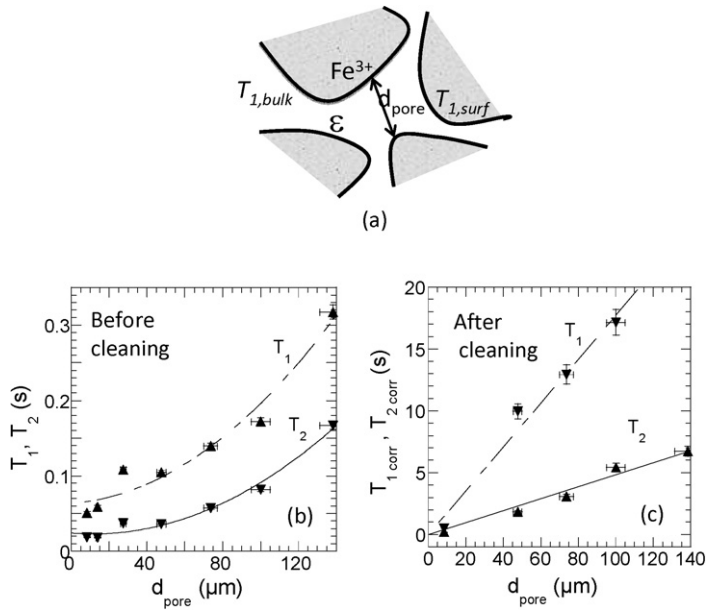

Fig. 1. (a) Schematic diagram of a porous media with indication of the relaxation variables used in the text. (b) The ^{1}H measured water spin–lattice (T_1) and spin–spin (T_2) relaxation times as a function of the pore diameter d_{pore}, at 2.2 MHz and 34 °C, before cleaning the surface (data from Ref. [13]). The quadratic continuous lines represent the best fits obtained with Eq. (2a). (c) The measured ^{1}H water spin–lattice (T_1) and spin–spin (T_2) relaxation times as a function of d_{pore}, at 2.2 MHz, and 34 °C after cleaning the surface (data from Ref. [13]). The lines represent the theoretical pore size dependences calculated with Eq. (2b), with the surface relaxivity parameters: $\rho_1 = 0.94$ μm/s and $\rho_2 = 3.4$ μm/s.

we describe the general situation, when both processes occur. We have considered explicitly the exchange rate W between the surface layer of thickness λ and the bulk, and their respective relaxation times $T_{1,surf}$ and $T_{1,bulk}$ [13]. One finds at long times t and under the condition of biphasic fast exchange [25], $t \gg T_{1,surf} \gg 1/W$, an exponential time decay of the longitudinal magnetization with the spin–lattice relaxation rate:

$$\frac{1}{T_1} = \frac{1}{T_{1,bulk}} + \frac{2\alpha\rho_1}{d_{pore}} \frac{1}{1 + \frac{\rho_1 d_{pore}}{4D}} \tag{1}$$

In Eq. (1), d_{pore} is the characteristic pore dimension (diameter) of the model pore and $\alpha = 1, 2$ or 3 is the shape factor for planar, cylindrical and spherical pore geometry, respectively. The efficiency of the surface spin–lattice relaxation rate is qualified by $\rho_1 = \lambda/T_{1S}$ and D is the translational self-diffusion coefficient within the pore. This length scale λ represents a representative distance over which the effects of the relaxation disappear. The dipole–dipole correlation being proportional to the inverse of the sixth power of the distance, λ is of the order of a few molecular sizes as was shown by some calorimetric measurements [26]. The expression of the spin–spin relaxation is similar, exchanging the indices 1 and 2. Eq. (1) shows clearly the independence of bulk and confined relaxation rates, while the confined rate depends on the two relaxation processes in series. A direct comparison of $4D/d_{pore}$ and $\rho_{1,2}$, shows that the slowest process limits the relaxation. For instance, when $4D/d_{pore} \ll \rho_{1,2}$ the relaxation is diffusion-limited, and Eq. (1) simplifies:

$$\frac{1}{T_{1,2}} = \frac{1}{T_{1,2bulk}} + \frac{8\alpha D}{d_{pore}^2} \tag{2a}$$

On the other hand when $4D/d_{pore} \gg \rho_{1,2}$, the relaxation is surface-limited, and one has:

$$\frac{1}{T_{1,2}} = \frac{1}{T_{1,2bulk}} + \frac{2\alpha\rho_{1,2}}{d_{pore}} \tag{2b}$$

These expressions thus relate directly the relaxation times T_1 or T_2 to either d_{pore}^2 or d_{pore} providing that the conditions of diffusion-limited or surface-limited relaxation are fulfilled, respectively. Eqs. (2a) and (2b) thus exhibit potentially two very different pore-size dependences that allow identifying the limiting relaxation process that occurs in pores.

2.2. Experimental transition between slow-diffusion and fast-diffusion relaxation processes in granular packings

We show by low field NMR relaxation that changing the amount of surface paramagnetic impurities leads to strikingly different pore-size dependences of the relaxation times T_1 and T_2 of liquids in pores. To evidence the net transition in the pore size dependences of the relaxation times T_1 and T_2 of liquids in pores between the surface-limited and diffusion

relaxation models, we have prepared a series of packings of non-porous SiC grains individually sorted in the range between 8 and 150 μm [13]. The interest of these samples is that they lead to those comparable of oil-bearing rocks. There is 25% of the surface covered by SiO_2. Two series of packings have been prepared before and after removing the surface paramagnetic impurities by hydrochloric acid cleaning. After cleaning, we evidence by Electron Spin Resonance (*ESR*) the quantity of chemically bonded Fe^{3+} paramagnetic ions. We measured at 2.2 MHz and 34 °C the pore-size dependence of spin–spin and spin–lattice relaxation times of water fully saturating these samples. Experimental results show that for the uncleaned porous media presenting a high surface density of paramagnetic impurities (Fig. 1b), T_1 and T_2 relaxation times of water vary as the square of the pore diameter d_{pore} (quasi-spherical pores). This dependence well agrees with the diffusion-limited relaxation (Eq. (2a) with $\alpha = 3$). On the other hand, the results show a linear pore-size dependence of T_{1corr} and T_{2corr} for the cleaned porous media, presenting a low surface density of paramagnetic impurities (Fig. 1c). Here $1/T_{1,2corr} = 1/T_{1,2} - 1/T_{1,2bulk}$. This dependence well agrees with the surface-limited relaxation (Eq. (2b)). We therefore estimate the surface relaxivity parameters $\rho_1 = 0.94$ μm/s and $\rho_2 = 3.4$ μm/s from the slopes of the linear fits of Fig. 1c. These values are typical of natural rock values, thus justifying that surface-limited relaxation process is relevant in these widely encountered porous systems.

3. Nuclear magnetic relaxation dispersion of surface spin–lattice relaxation rate

3.1. Theory

In the fast diffusion limit, one can apply the biphasic fast exchange model [25] where the exchange time between the surface and the bulk phases is shorter than their respective relaxation times, the overall proton relaxation rate $1/T_1$ is a linear combination of a bulk $1/T_{1,bulk}$ and a surface relaxation rate $1/T_{1,surf}$. We show here that the surface term is a superposition of the contribution $1/T_{1,2D}$ of the proton species diffusing in the proximity of the fixed paramagnetic species [11] and the contribution $1/T_{1,param}$ of the proton species linked to the first coordination sphere of paramagnetic centers [27,28]:

$$\frac{1}{T_1(\omega_I)} = \frac{1}{T_{1,bulk}} + \frac{N_{Surface}}{N}\frac{1}{T_{1,2D}(\omega_I)} + \frac{N_{param}}{N}\frac{1}{T_{1,param}(\omega_I)} \tag{3}$$

The bulk relaxation term, $1/T_{1,bulk}$, has no proton Larmor frequency $\omega_I/2\pi$ dependence in the range studied here [29]. The two surface relaxation terms are highly sensitive to the local physical-chemistry effects at the pore surface resulting in different frequency behaviors in disconnected ranges. The inclusion of the nuclear paramagnetic term is new and critical because it extends the theory to make the NMRD of protic liquid different to the aprotic one. The terms protic and aprotic are defined through the ability of the liquids studied to exchange or not their protons, respectively, this exchangeable character being independent of the polarity of such liquids. For instance, the protic liquid is revealed in presence of a possible hydrogen bonding. The aprotic liquid exists in presence of non-exchangeable protons as in $-CH_3$ or $-CH_2$ groups. We outlined below the calculation of these two terms in the local layer geometry at proximity of the pore surface (Fig. 2). In this model, $N_{Surface}/N = \lambda S_P \rho_{liquid}$ is the ratio between the number $N_{Surface}$ of liquid molecules diffusing within the thin transient layer λ close to the pore surface and the bulk liquid population N. Here λ is of the order of a few molecular sizes [26]. S_p is the specific surface area of the sample and ρ_{liquid} is the density of the proton liquid. $N_{param}/N = (N_{param}/N_S)(N_S/N) \ll N_S/N$ is the ratio between the number of liquid molecules bonded to the paramagnetic sites at the surface and in the bulk.

The paramagnetic sites located at the pore surface have a ligand field which either traps a moving proton species defined as a *protic* liquid wetting the surface (Fig. 2), or does not trap a moving proton species defined as an *aprotic* liquid. These chemical behaviors result in two distinct features of the NMRD that can be individualized by $1/T_{1,2D}(\omega_I)$ or $1/T_{1,param}(\omega_I)$ in Eq. (3).

We first consider the case of $1/T_{1,2D}(\omega)$ corresponding to proton bearing aprotic liquid diffusing in proximity to the solid liquid interface in a porous medium, *i.e.* the proton species is not trapped in the ligand field of a paramagnetic site. This allows one not to consider the $1/T_{1,param}(\omega_I)$ contribution in Eq. (3). We consider also the presence of a very small quantity of fixed paramagnetic species of spins, S, uniformly distributed on these surfaces with a surface density, σ_s. Because the magnetic moment of the paramagnetic species is large ($\gamma_S = 659\gamma_I$), there is no ambiguity about the relaxation mechanism of the diffusing proton spins, I, which is the intermolecular dipolar relaxation process induced by fixed spins, S, and modulated by the translational diffusion of the mobile spins, I, in close proximity to these surfaces. Basically, the nuclear spin–lattice relaxation rate of the diffusing spins I, in proximity to the S spins, is given formally by the general expression [29]:

$$\frac{1}{T_{1,2D}(\omega_I)} = \frac{2}{3}(\gamma_I\gamma_S\hbar)^2 S(S+1)\left[\frac{1}{3}J_L^{(0)}(\omega_I - \omega_S) + J_L^{(1)}(\omega_I) + 2J_L^{(2)}(\omega_I + \omega_S)\right] \tag{4}$$

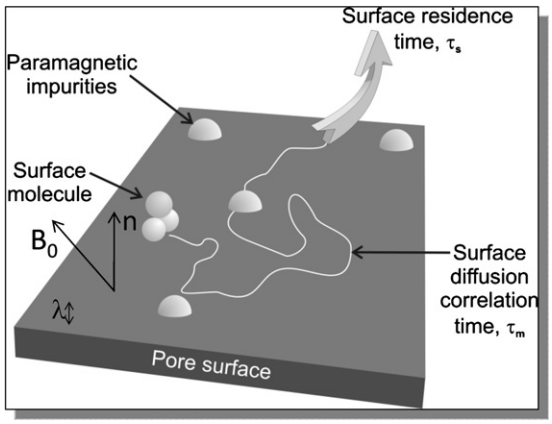

Fig. 2. Schematic diagram of surface diffusion of the proton species of an aprotic liquid on a pore silica surface limited by exchange with bulk liquid.

where $J_L^{(m)}(\omega)$ $(m \in \{-2,+2\})$ are the spectral densities in the Laboratory frame (L) associated with the constant magnetic field $\boldsymbol{B}_0$ expressed at the Larmor frequencies of the electron and proton related by $\omega_S = 658.21\omega_I$ and defined as the exponential Fourier transforms:

$$J_L^{(m)}(\omega) = \int_{-\infty}^{+\infty} G_L^{(m)}(\tau) e^{-i\omega\tau}\,\mathrm{d}\tau \tag{5a}$$

of the stationary pairwise dipolar correlation functions $G_L^{(m)}(\tau)$ $(m \in \{-2,+2\})$ given by:

$$G_L^{(m)}(\tau) = \left\langle F_L^{(-m)}(t) F_L^{(-m)*}(t+\tau)\right\rangle \tag{5b}$$

Eq. (5b) describes the persistence of the autocorrelation of the dipole–dipole interaction $F_L^{(m)}(t) \sim 1/r_{IS}^3(t)$ between the magnetic moments associated with the spins I and S and modulated by the translational diffusion during a short time interval τ of spins I at distance r_{IS} of a paramagnetic spins S fixed on the pore surface. The notation $\langle\ldots\rangle$ stands for the ensemble average over all the positions of the spins I at time 0 and τ for a given density σ_S of spins S. This ensemble average can be expressed as an integral average over the normalized diffusive propagator $P(\vec{r}_0,\vec{r},\tau)$:

$$G_L^{(m)}(\tau) = \int \mathrm{d}\vec{r}_0\, p(\vec{r}_0) F_L^{(-m)}(0) \int \mathrm{d}\vec{r}\, P(\vec{r}_0,\vec{r},\tau) F_L^{(-m)*}(\tau) \tag{6}$$

Here $P(\vec{r}_0,\vec{r},\tau)$ is a solution of a diffusive equation with initial and boundary conditions and $p(\vec{r}_0) = \sigma_S/\lambda$ represents the equilibrium and uniform density of spin pairs I–S at equilibrium.

We have detailed in Ref. [11] all the calculations of the correlation functions $G_L^{(m)}(\tau)$ and spectral densities $J_L^{(m)}(\omega)$ within the following conditions: (i) We use the well-known properties of rotation of spherical harmonics in different bases to facilitate the calculations in the lamellar frame (M) of Fig. 2 before coming back to the laboratory frame (L) associated to the constant direction of the magnetic field $\boldsymbol{B}_0$. (ii) We use the anisotropic dynamical model presented in Fig. 2 with an unbounded and isotropic diffusion perpendicular to the normal axis $\boldsymbol{n}$ and a bounded diffusion along such an axis. (iii) The pairwise dipolar correlation functions $G_L^{(m)}(\tau)$ have been estimated at times τ much longer than the transverse diffusion correlation time $\tau_m = \delta^2/(4D_{I\perp})$ where δ is the molecular size of the I spin-bearing molecule with a translational diffusion coefficient $D_{I\perp}$ in direction perpendicular to $\boldsymbol{n}$. (iv) We introduce the effects of the finite time of residence $\tau_S \gg \tau_m$ at pore surface by an exponential cut-off in the time dependence of the I–S pair correlations. (v) A powder average of $J_L^{(m)}(\omega)$ over all the orientations of the $\boldsymbol{n}$ direction relative to the constant direction of the magnetic field $\boldsymbol{B}_0$ has been done. These calculations lead, at low frequency, to the following overall spin–lattice relaxation rate of the 2D diffusion of liquid diffusing in proximity to the pore surface:

$$\frac{1}{T_1(\omega_I)} = \frac{1}{T_{1,bulk}} + \frac{\pi\lambda S_P \rho_{liquid}\sigma_S(\gamma_I\gamma_S\hbar)^2 S(S+1)\tau_m}{15\lambda^2\delta'^2(1+x^2)}\left[3\ln\left(\frac{1+\omega_I^2\tau_m^2}{\tau_m^2/\tau_S^2+\omega_I^2\tau_m^2}\right)+7\ln\left(\frac{1+\omega_S^2\tau_m^2}{\tau_m^2/\tau_S^2+\omega_S^2\tau_m^2}\right)\right] \tag{7}$$

In Eq. (7), $x = \delta/\delta'$ is a parameter introduced for taking into account a variable distance δ' of minimal approach between I and S spins compared to the molecular size δ of the studied moving liquid. $S = 5/2$ for the spins of Fe^{3+} or Mn^{2+} paramagnetic ions of surface concentration $\sigma_S = (\eta_S\rho_{solid}\xi)$, where η_S is the volume concentration of paramagnetic ions measured by *ESR*, $\xi \sim 0.5$ nm is a thin layer of paramagnetic ions corresponding to the lattice constant of the solid structure at proximity of the pore surface and ρ_{solid} is the density of the solid material. Eq. (7) has a bilogarithmic frequency

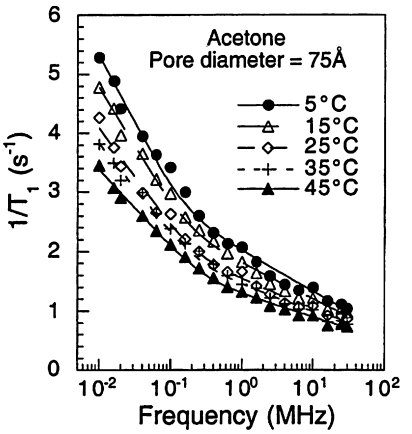

Fig. 3. Magnetic-field dependences of ^{1}H spin–lattice relaxation rates of aprotic acetone embedded in a packed samples of calibrated porous glasses beads at 5, 15, 25, 35, and 45 °C (data from Ref. [11]). The continuous lines correspond to the best fits to Eq. (7) as discussed in the text.

dependence (proton Larmor frequency ω_I and electronic frequency $\omega_S = 659\omega_I$ due to the numerous 2D molecular reencounters between spins I and S occurring within the thin transient layer λ). Eq. (7) contains also two correlation times: the translational correlation time, τ_m, associated with individual molecular jumps in proximity to the surface and the surface residence time, τ_s, which is limited by the molecular desorption from the thin surface layer λ. τ_s controls how long the proton species I and the Fe^{3+} or Mn^{2+} ion S stay correlated. It depends on both the strength of the chemical bonds and the re-occurrence of first neighbor interactions induced by the fluid confinement in pores.

3.2. NMRD experiments on calibrated microporous silica glasses

The magnetic-field dependence of the proton spin–lattice relaxation rates for suspensions of 75 Å chromatographic and calibrated glass beads are reported for fields corresponding to ^{1}H Larmor frequencies from 0.01 to 30 MHz over a range of temperature from 5 to 45 °C for aprotic acetone solvent (Fig. 3) [11]. A common feature of these data is that the relaxation rate has a bilogarithmic dependence on the Larmor frequency, in agreement with Eq. (7). The iron content of these samples, checked by electron spin resonance (*ESR*) and analytical chemistry measurements, is 45 ppm for the 75 Å pore glasses. This is sufficient to provide a dominant relaxation path for the proton spins at low magnetic-field strengths. From the specific area of the glass and if we assume a uniform volume density of paramagnetic species, the surface density σ_S of paramagnetic centers is 3.463×10^{11} Fe/cm^2. The average distance between the paramagnetic centers is then on the order of $1/\sqrt{\sigma_S}$, which is 170 Å for the 75 Å glass samples. These figures provide an estimate of the range for the persistence length of the two-dimensional character sensed by the magnetic relaxation of the proton spins induced by the paramagnetic center. The good fitting with the bilogarithmic frequency dependence of Eq. (7) obtained at different temperatures for the nuclear magnetic dispersion data of Fig. 3 proves the validity of the proposed model. From individual fit, one deduces a value of the surface translational correlation time τ_m whose temperature dependence is typical of an activated diffusive process. It is important to note that Eq. (7) was derived without an explicit inclusion of the electron–spin relaxation rate as a potential source of important fluctuations in the electron–nuclear coupling. Were the electron–spin relaxation time sufficiently short that it competed with the translational diffusion times, then the low-field portion of the relaxation dispersion would be independent of field strength [26,27], which is not consistent with observation. Thus the neglect of the electron–spin relaxation in Eq. (3) is supported by the experimental result.

4. Continuous multi-scales NMR relaxation investigation of microstructure evolution of cement-based materials

Concrete is a construction material composed of cement (commonly Portland cement) as well as aggregates, sand, water and chemical admixtures such as silica fume and adjuvants. Concrete solidifies and hardens after mixing with water and placement due to a chemical process known as hydration. The water reacts with the anhydrous cement, which bonds the other components by hydrates and forms a hardened cement paste known as the main ingredient of concrete. The important mechanical and durable performances of concrete are mainly due to the high compactness of this material but also to the microstructure of hydrated cement paste. Here the microstructure includes different mesoscopic properties such as: porosity, specific surface area, distribution and connectivity of pore sizes as well as tortuosity factor. Questions still exist about the microstructure of such a highly disordered and multiscale hydrated cement paste. Answering these questions is important because the microporous features influence the mechanical properties of materials as well as the transport efficiency of water and aggressive agents. A better control on the appearance and evolution of the microstructure during the hydration and setting is still needed to improve these properties. This is important because more than a cubic meter per human being on earth is produced each year that makes concrete the world's most widely used manufactured material.

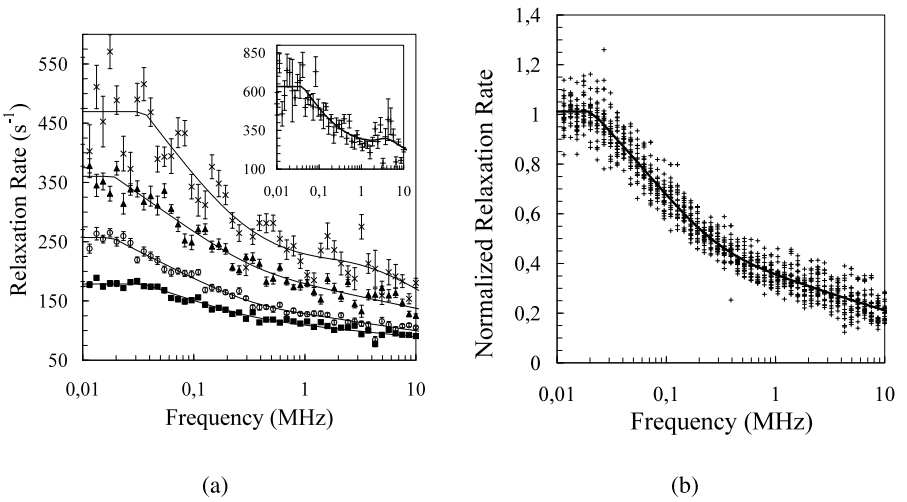

Fig. 4. (a) Measured water ^{1}H spin–lattice relaxation rates of a hydrated mortar at a water to cement ratio, $w/c = 0.38$, as a function of the proton Larmor frequency, for different duration of hydration: 0h34 (■), 7h27 (○), 8h45 (▲) and 9h40 (×), upwards (data from Ref. [16]). The insert represents the data obtained after a hydration time of 10h32 (+), the labels for the two axis are equivalent to those of the main figure. The continuous lines correspond to the best fits obtained with equations given in Ref. [16]. (b) Renormalization of the data obtained in (a) for all hydration times.

Here, we just outline some of our recent non-invasive NMR and low field nuclear spin relaxation approaches to investigate the evolution of the microstructure of various cement-based materials in various conditions.

As a typical first example of a cement-based material, we consider a reactive powder mortar sample prepared by mixing cement, sand, silica fume, water and superplasticizer with a water to cement ratio $w/c = 0.38$. Before addition of water, the specific surface area of the various grains is very low whereas after the dissolution–precipitation process, calcium silicate hydrate structures (CSH) appear at the surface of the grains leading to a very high surface area that increases continuously with time. We used the nuclear magnetic relaxation dispersion (NMRD) [7,8], the measurement of the longitudinal relaxation rate R_1 as a function of magnetic field strength or nuclear Larmor frequency of water confined within the hydrated cement. The benefit of exploring here the range of low frequency is to isolate the typical NMRD dispersion features of $1/T_1$ associated to the different processes of molecular surface dynamics. An original model based on solid/liquid cross-relaxation, proton surface diffusion and nuclear paramagnetic relaxation, in presence of progressive hydration, is proposed to interpret the remarkable features of the proton NMRD profiles [16,18]. We present in Fig. 4a, the proton NMRD data obtained for increasing duration of hydration for such a mortar. Measurements are performed, at a temperature stabilized at 25 °C, on a fast field cycling spectrometer from Stelar Company. The NMRD dispersion profiles, shown in Fig. 4a, have been obtained for fifty different measured field values between 0.01 and 10 MHz. An individual NMRD profile is obtained in twenty minutes or so. This is sufficiently rapid to follow the hydration of the mortar every thirty minutes during the first twelve hours. We evidence by Electron Spin Resonance (*ESR*) a quantity of $\eta_S = 1.17 \times 10^{19}$ paramagnetic Fe^{3+} ions per gram of dry material. Assuming a uniform distribution, we deduce a proportion of surface Fe^{3+} impurities, $\sigma_S = \eta_S \rho_{solid} \xi$, to which relaxation of liquid protons of the saturated porous media is sensitive. Here $\rho_{solid} = 2.5$ g/cm^3 is the density of the solid material and $\xi = 6$ Å is the average inter-layer distance between two Fe^{3+} ions. The surface density of Fe^{3+} impurities thus becomes $\sigma_S = 1.8 \times 10^{12}$ Fe^{3+}/cm^2, and is independent of S_p. We note three remarkable features in the ^{1}H NMRD of water in hydrated mortars (Fig. 4a): (i) There is a plateau below a cross-over frequency $\omega_c \sim 22$ kHz; (ii) Above ω_c, one observes a bilogarithmic dispersion behavior, characterized by a 10/3 slope ratio, for every duration of hydration. This frequency behavior is unambiguously consistent with a two-dimensional proton–water diffusion at proximity of the paramagnetic relaxation centers (see Eq. (7)); (iii) Between 3 and 5 MHz, one notes an enhancement of the relaxation after 10 hours of hydration. A renormalization of the ^{1}H NMRD data collected for all durations of hydration has been achieved by subtracting the limiting constant bulk relaxation rate at high frequency and dividing the resulting data by the value of the respective low frequency plateau (Fig. 4b). This renormalization proves that the same nuclear magnetic relaxation process occurs for all duration of hydration. Moreover, such a renormalization (Fig. 4b) has allowed us to measure the surface diffusion translational correlation time $\tau_m = 0.7$ ns that gives a surface diffusion coefficient about two order of magnitude less than the surface diffusion coefficient of water in bulk. We measured a universal value $\tau_m = 1$ on several different cement-based materials including reactive powder concrete. This clearly shows that nuclear spin relaxation is able to sense the translational dynamics of proton species at surface of CSH pores that are present in all these materials. The unique cross-over frequency ω_c is indicative of a fundamental modification in the relaxation when the correlation time reaches the value $\tau_c \sim 1/\omega_c = 7.2$ µs.

Another representative model cement-based material is the synthesized tricalcium silicate Ca_3SiO_5 (the so-called C_3S) which represents 60–70% of industrial Portland cement. Fig. 5 shows the NMRD curves $1/T_1 = f(\omega)$ obtained on an one

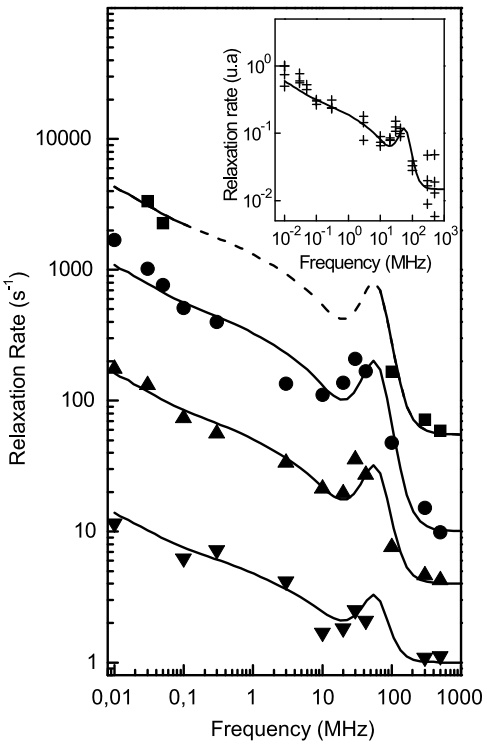

Fig. 5. Logarithmic plot of the dispersion NMRD profiles showing the four longitudinal relaxation rates $1/T_1$ versus the external magnetic field expressed in terms of the Larmor frequencies of the proton for a C_3S paste hydrated one year with $w/c = 0.4$ at room temperature (data from Ref. [17]). The four curves have been successfully rescaled in the inset. The continuous lines correspond to the best fit obtained by the relaxation model given in Ref. [16].

year aged C_3S sample [17] with different spectrometers whose frequency ranges between 10 kHz and 500 MHz. The renormalization of all these dispersion curves to a single one, shown in the inset of Fig. 5 proves that the same relaxation process occur at each of the four classes of $1/T_{1i}$ from 1 to 4000 s^{-1}. The solid lines in Fig. 5 are the best fits obtained with Eqs. (3)–(7). The four NMRD curves being mainly due to the surface contribution (Eq. (7)), that is weighted by the surface to volume ratio of the pores, these data gives the following average pore sizes $\langle R_i \rangle$: 1.8, 7.0, 50 and 600 nm.

We have also used the nuclear spin relaxation method to probe directly the surface area of a hydrated cement-based material that do not require any drying or temperature modification [16]. We have discussed above why the surface contribution in Eq. (7) is dominant at low frequency in comparison with the frequency independence of the bulk contribution in this frequency range. To obtain the specific surface area of the cement paste and prevent the kinetics effects occurring during the acquisition of the complete NMRD profile, we focus only on the measurement of the time evolution of the proton–water $1/T_1(t)$ at 10 kHz which is on the plateau of the profile in Fig. 4. The method, which can be performed at room temperature, is sensitive to both open and closed porosity in a wide range of length-scales. This allows probing directly the surface area and proton species surface dynamics of different cement-based materials from the NMRD data. The method is sufficiently rapid to be applied continuously during the progressive hydration and setting of cement. At this low frequency, we have shown [16,18] that the overall relaxation is mainly due to the liquid proton species in cross correlation with the solid protons at the still growing CSH surfaces. We have displayed in Fig. 6 the time evolution of the specific surface area of a white cement paste up to the first 100 hours of hydration [18]. Similarly to the well-known calorimetric measurement, Fig. 6 shows the three periods of the cement hydration, namely the dormant period at the beginning, the setting due to the advancement of chemical reaction after 4 hours and then the transition to the slower diffusive period at long times. It is well known that the calorimetric measurement gives a master curve for getting the degree of advancement of the chemical reaction at the origin of the hydration process. We show here that the time evolution of the remaining water protons $1/T_1(t)$ at 10 kHz displayed in Fig. 6, gives another master curve that reveal the decrease of the water dynamics at proximity of a time growing solid surface of the CSH hydrates.

Last, the recent applications of 2-dimensional T_1–T_2 (Fig. 7a) and T_2-z-store-T_2 (Fig. 7b) correlation experiments [19] and [20] are now briefly described. These experiments confirm the discrete pore size distribution observed and have provided the first clear evidence (by the presence of cross peaks in Figs. 7a and 7b of a chemical exchange of water protons between the connected gel micropores). The T_2-z-store-T_2 experiment has two significant advantages over the T_1–T_2 experiment. First, it clearly identifies and correlates measurements in two intervals, t_1 and t_3, that are separated in time by a third interval, t_{store}. It is therefore more straightforward to consider that there is an exchange period during which the proton species are moving between reservoirs. Second, the off diagonal peaks can be assigned unambiguously to exchange.

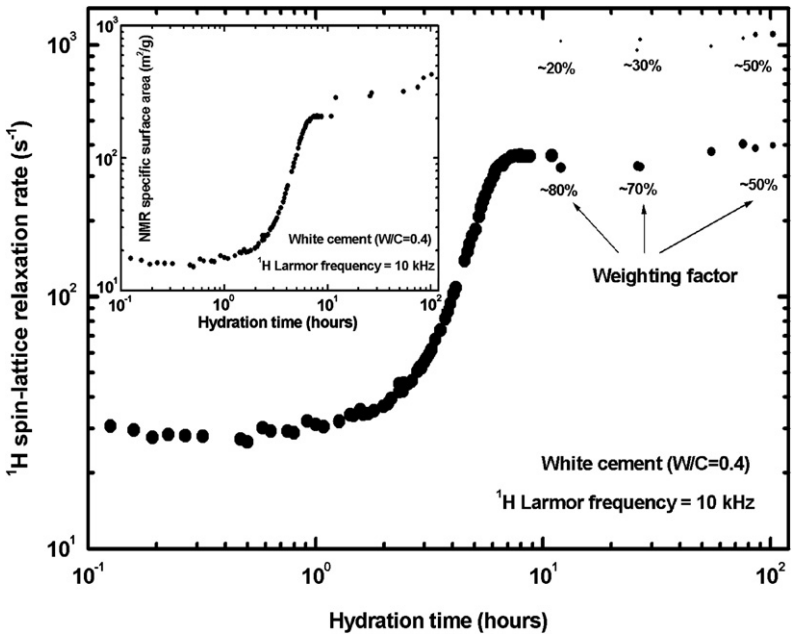

Fig. 6. ^{1}H spin–lattice relaxation rate of a white cement paste hydrated with $w/c = 0.4$ as a function of the hydration time measured at a Larmor frequency of 10 kHz in white cement (data from Ref. [18]). The weighting factors for each of the relaxation components are indicated. The inset represents the NMR specific surface area deduced from the data in the main figure with use of equations given in Ref. [18].

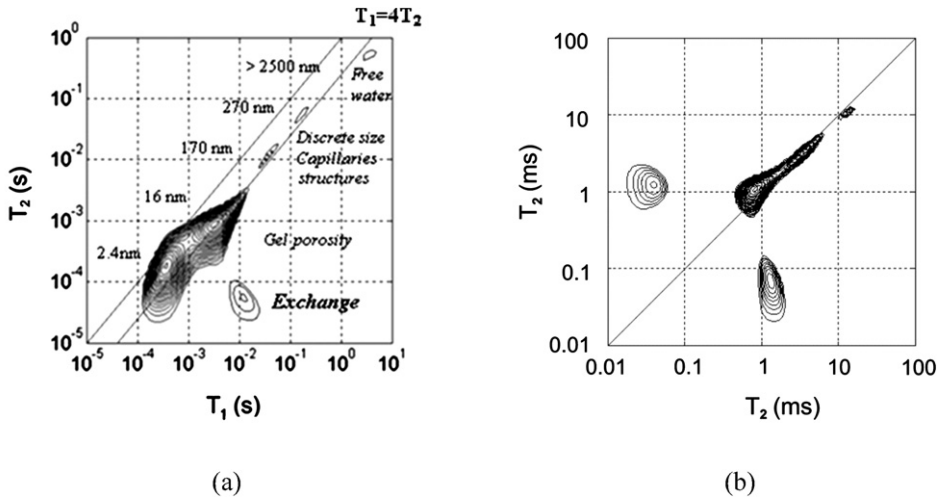

Fig. 7. (a) The 2D spin-correlation spectrum T_1–T_2 of a white cement sample cured for 4 days (data from Ref. [19]). A series of discrete features lie along the line $T_1 = 4T_2$ parallel to the diagonal. Both this line and the principal diagonal $T_1 = T_2$ are shown as dotted lines. There is an off-diagonal feature at the position $T_1 = 10$ ms and $T_2 = 50$ ms. The intensity contours (arbitrary units) are equally spaced up from a zero base. (b) Experimental 2D spin-correlation spectrum T_2-z-store-T_2 for a white cement paste with water-to-cement ratio 0.4 and three days old. The storage time is 10 ms (data from Ref. [20]). There are two cross peaks that evidences an exchange process between connected micropores.

If there is no exchange, then there are no off-diagonal peaks. The *ESR* calibration of the pore sizes suggests that the two primary relaxation reservoirs seen both comprise rather small pores. The smallest pore radius is *circa* 1.2 nm. This is consistent with estimates to be found in the literature of the CSH inter-planar spacing which range from 0.9 to 1.2 nm [30]. However, the second significant reservoir suggests a radius of 9–27 nm, dependent on pore shape. This is much smaller than the expected size of capillary pores. We therefore suggest that the two observed reservoirs may be attributed to alternate gel structures. One possibility is that the smaller pore size reservoir is associated with inner product, the larger with outer product, both created as the material hydrates. The exchange rate between these structures has been estimated to be 5 ms^{-1}. From this, water diffusivity within the CSH structures has been calculated that broadly corresponds to the results of molecular dynamic simulations in related systems [31].

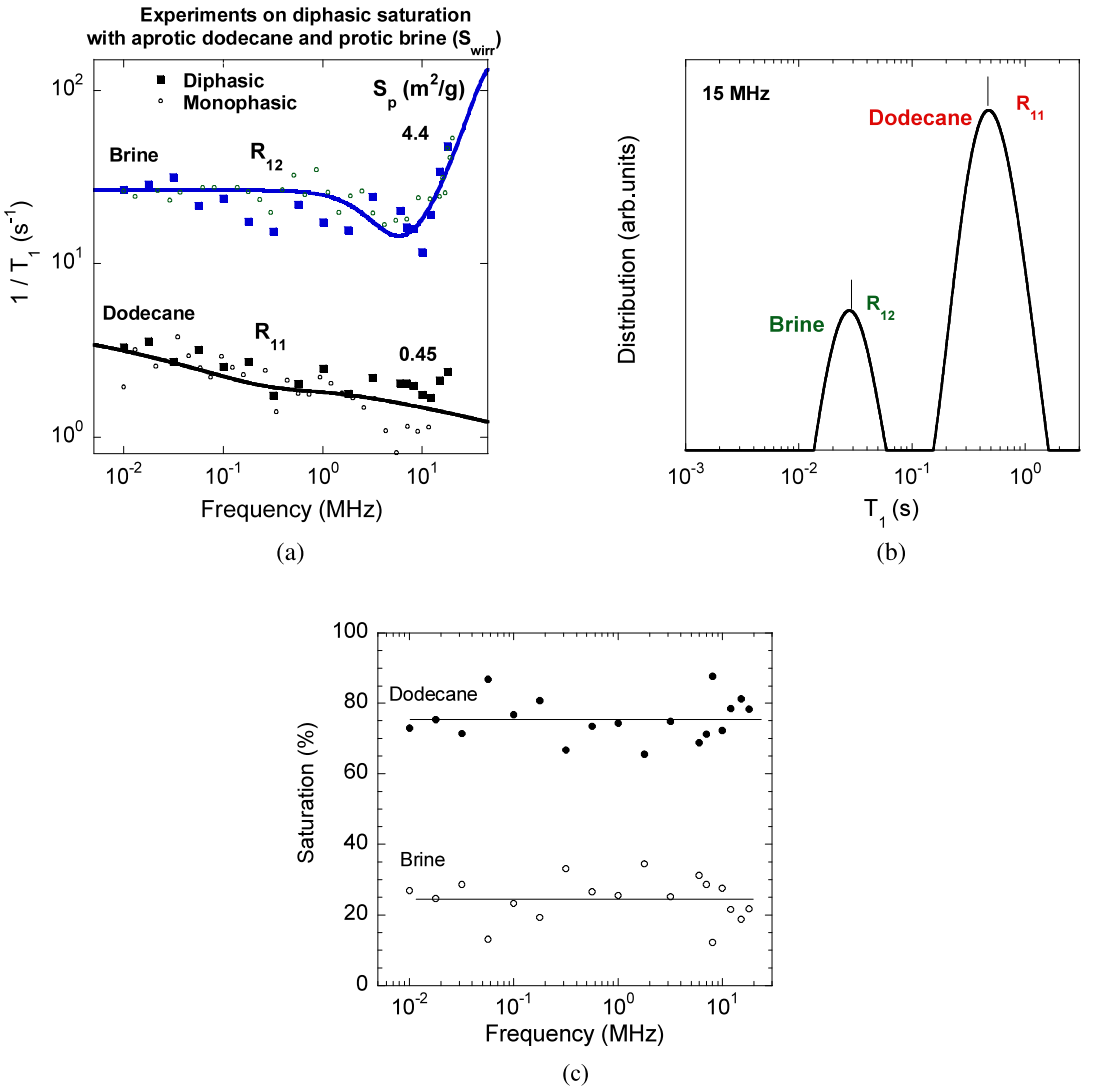

Fig. 8. (a) Logarithmic plot of the dispersion NMRD profiles of carbonate rock saturated with both dodecane and 50 kppm NaCl brine ($S_{w,ir}$) (data from Ref. [15]). The continuous lines were obtained from Eqs. (6), (7) of Ref. [15] for dodecane (aprotic liquid) leading to the surface dynamical affinity $A = 130$ and from Eqs. (8)–(10) for wetting brine (protic liquid) of Ref. [15]. The relaxation rates of the mixture (large full dots) are compared with the rates R_{11} and R_{12} (small empty dots) obtained with monophasic saturations of dodecane and brine, respectively. (b) Dual porosity observed through the T_1 distribution obtained by the 1D Laplace inversion of the longitudinal magnetization decay at 15 MHz. The vertical ticks represent the two T_1 values deduced from our own iterative approach. The comparison with the NMRD data allows to identify the nature of the liquid saturating individual pore. (c) Frequency dependence of the saturation (%) of brine and dodecane that is conserved in the whole frequency range studied. This saturation has been obtained by integration of the bimodal distribution obtained at each frequency.

5. Dynamical surface affinity of diphasic liquids as a probe of wettability of multimodal macroporous rocks

Wettability is the ability of a fluid to spread onto a solid surface in the presence of other immiscible fluids. It is relevant in fundamental interfacial phenomena underlying coating, bonding, adhesion and other related effects in porous media. For instance, the wettability of a rock/oil/brine system affects fluid saturation, capillary pressures, electrical properties and relative permeabilities [32,33]. Wettability of fluids in oil and gas reservoirs has a direct effect on efficiency of hydrocarbon recovery. In most cases massive water injection is performed to move oil toward the production zones, and if wettability variations occur the water has the tendency to flow in the water wet locations leaving oil in place in oil-wet locations. Due to its economical impact, control and monitoring of wettability *in situ* justify huge investments in core analysis for laboratory measurements.

Techniques able to map wettability in the field are still not developed. Measurements on cores require long and tedious preparation, and never reflect the actual state of wettability. These cores are generally not tested in their native state. They are cleaned and saturated with known brine and oil. They are aged and tested in spontaneous drainage (oil in water

saturated core) and imbibition (water in oil saturated core). An *Amott* index is then determined (from 1 for water wet rocks to -1 for oil wet cores) [34]. A contingent method called USBM (U.S. Bureau of Mines) uses pressure gradient to force the flow of oil in the core saturated with water and reciprocally to force the flow of water in the core saturated with oil [34]. The USBM index (varying for $-\infty$ to $+\infty$) is based on the logarithm of the ratio of energy required to move oil with water versus the energy required to move water with oil. Both Amott and USBM methods are accepted as a standard by industry, however they do not completely compare in all cases [35]. A more recently introduced NMR T_2 index [36–38] expresses the total surface of rock wetted by water minus the total surface of rock wetted by oil and divided by the total surface in contact with the fluid. This method uses the fact that a fluid surrounded by a wetting fluid shows a T_2 relaxation distribution of a bulk fluid, whereas a fluid in contact with the rock exhibits a shorter T_2 due to the confinement by the surface. This method has some limitations since it requires a measurement at complete water saturation and also requires the knowledge of the T_2 shape of the oil in bulk conditions. None of these techniques allow the local probing of interaction between the fluid and the rock-pore surface in a single non-invasive measurement.

Here, we have proposed again to use nuclear magnetic relaxation dispersion (NMRD) to probe the dynamical surface affinity of diphasic liquids as a measurement of wettability [15]. This technique measures proton $1/T_1$ over a large range of applied magnetic fields and yields unique information about the extent to which a fluid is dynamically correlated with a solid rock surface. Unlike conventional transverse relaxation studies, this approach is a direct probe of the dynamical surface affinity of fluids. We show that the low-frequency dispersion of the proton spin–lattice relaxation rates $1/T_1$ of aprotic (oil) and protic (water) diphasic liquids can provide their relative wettabilities in porous media with complex pore size distribution (multimodal). The use of aprotic and protic liquids allows studying the physical chemistry effects that matters at pore surface such as binding effects with paramagnetic metallic ions or proton exchange with surface groups.

We predict theoretically the specific NMRD features of aprotic liquids diffusing in the proximity of paramagnetic relaxation sites at pore surfaces and protic liquids bounded to these sites [15]. To quantify these features we introduce a microscopic dynamical surface affinity index which measures the dynamical correlation (*i.e.* the microscopic wettability) between the diffusive fluid and the fixed relaxation sources at the pore surfaces. This affinity index is defined as the ratio, $A = \tau_S/\tau_m$, of the time of residence of the moving proton species at the pore surface by the translational correlation time, τ_m, associated with individual molecular jumps in proximity to the surface. This ratio thus represents roughly the number of hopping jumps on the surface. We apply, for the first time, this non-invasive *in situ* method to carbonate reservoir rocks of bimodal porosity which are known to hold about two thirds of the world's oil reserves [15]. We confirm experimentally the predictions of the relaxation features for aprotic and protic liquids as well as pore-size dependence of wettability. The *in situ* results obtained on carbonates of bimodal porosity saturated with an oil/brine mixture reveal unambiguously the pore size dependence of wettability.

6. Conclusion

Various one and two-dimensional low-field NMR relaxation techniques were described to characterize the structure and molecular dynamics of liquids in confined environments. We focused mainly on high surface area materials including calibrated porous silica glasses, granular packings, cement based materials and natural porous rocks. In each case, we have briefly outlined the necessary modelling to interpret the multi-scaled NMR data.

We have particularly insisted in the nuclear magnetic relaxation dispersion (NMRD) on cement pastes and other cement-based materials. From these experiments a quantitative method is proposed to characterize the time evolution of the microstructure of cement paste on different lengthscales between 2 and 500 nm. This method allows one to follow the progressive setting of the pore size distribution that evolves, after completion of hydration, to an equilibrium state characterized by a power-law representative of a hierarchical order that stabilizes after four months the same texture on different lengthscales. This distribution is characteristic of a surface distribution where $D_f \approx 2.6$ is the surface fractal dimension that takes into account the hierarchical order in the texture of the material. Similarly NMRD technique gives a continuous and direct measurement of surface dynamics of proton species τ_m and specific surface area $S_{p,NMR}$ of various cement-based materials. This technique allows a clear separation of the NMRD of mobile water at the surface of the pores from that of the bulk. Though $S_{p,NMR}$ ranges within the results of most other techniques, there are several advantages in favor of our measurements: (i) Proton NMRD is neither invasive nor destructive because one measures the response of the mixing water itself in the normal saturated state of cement. No liquid or gas intrusion, no drying or other temperature and pressure modifications are required that risk damaging the microstructure; (ii) The measurement is sufficiently fast to be applied continuously during the progressive hydration and setting of the material; (iii) The remarkable features of the proton NMRD at low frequency allow one to probe directly the proton surface dynamics that contribute to $S_{p,NMR}$. The technique has also been applied to characterize the average pore sizes and distribution. Last, T_1–T_2 and T_2-store-T_2 nuclear 2D spin correlation measurements in cements have been outlined. These experiments confirm the discrete pore size distribution observed and have provided the first clear evidence for chemical exchange of water protons between connected gel micropores. These experiments have also provided further evidence in support of the 2-dimensional surface diffusion model of spin-relaxation in cements. Last, the T_2-store-T_2 2D spin correlation experiment confirms the existence of a water exchange between connected micropores with an estimated rate of 5 ms^{-1}. From this water diffusivity within the C–S–H structures has been calculated that broadly corresponds to the results of molecular dynamic simulations in related systems.

Finally, we have presented a new and non-invasive method for probing wettability of rock/oil/brine systems using nuclear magnetic relaxation dispersion (NMRD). Unlike conventional transverse relaxation studies, this approach gives a direct probe of the dynamical surface affinity of fluids, thus allowing the separation of wetting from non-wetting fluids through their typical NMRD features. To quantify these features we introduce a microscopic dynamical surface affinity index which measures the dynamical correlation (*i.e.* microscopic wettability) between a diffusive fluid and fixed Mn^{2+} paramagnetic relaxation sources at the pore surfaces. For the first time, we have applied this technique to carbonate reservoir rocks of bimodal porosity saturated with a mixture of dodecane and 50 kppm NaCl. The experimental NMRD results obtained on carbonate core plugs of bimodal porosity saturated with this oil/brine mixture clearly discriminate the wetting behavior of the fluids in the pore system. The data have been processed using a proposed model that clearly reveals the pore size dependence of wettability. Here the typical shapes of the two separated NMRD profiles allows us to conclude that water stays in the small pores while oil is on the large ones. This proves the existence of a flow path between the large pores that does not involve the small ones.

Acknowledgements

J.-P. Korb thanks for their collaborations and discussions D. Petit and P. Levitz (École polytechnique, Palaiseau); P.J. McDonald and J. Mitchell (University of Surrey) and A. Plassais, N. Lequeux, C. Porteneuve (ESPCI, Paris).

References

[1] F. d'Orazio, S. Bhattacharja, W. Halperin, K. Eguchi, T. Mizusaki, Phys. Rev. B 42 (1990) 9810.
[2] J.Y. Jehng, PhD thesis, Northwestern University, 1995.
[3] G. Liu, Y. Li, J. Jonas, J. Chem. Phys. 95 (1993) 6892.
[4] J.-P. Korb, Shu Xu, J. Jonas, J. Chem. Phys. 98 (1993) 2411.
[5] J.-P. Korb, A. Delville, Shu Xu, G. Demeulenaere, G. Costa, J. Chem. Phys. 101 (1994) 7074.
[6] J.-P. Korb, L. Malier, F. Cros, Shu Xu, J. Jonas, Phys. Rev. Lett. 77 (1996) 2312.
[7] A.G. Redfield, W. Fite, H.E. Bleich, Rev. Sci. Instrum. 39 (1968) 710.
[8] F. Noack, Bull. Ampere 175 (1994) 18.
[9] R. Kimmich, H.W. Weber, Phys. Rev. B 47 (1993) 11788.
[10] M. Whaley, A.J. Lawence, J.-P. Korb, R.G. Bryant, Solid State Nucl. Magn. Reson. 7 (1996) 247.
[11] J.-P. Korb, M. Whaley-Hodges, R.G. Bryant, Phys. Rev. E 56 (1997) 1934.
[12] J.-P. Korb, M. Whaley-Hodges, Th. Gobron, R.G. Bryant, Phys. Rev. E 60 (1999) 3097.
[13] S. Godefroy, J.-P. Korb, M. Fleury, R.G. Bryant, Phys. Rev. E 64 (2001) 021605.
[14] S. Godefroy, M. Fleury, F. Deflandre, J.-P. Korb, J. Phys. Chem. B 106 (2002) 11183.
[15] J.-P. Korb, G. Freiman, B. Nicot, P. Ligneul, Phys. Rev. E 80 (2009) 061601.
[16] F. Barberon, J.-P. Korb, D. Petit, V. Morin, E. Bermejo, Phys. Rev. Lett. 90 (2003) 116103.
[17] A. Plassais, M.-P. Pomiès, N. Lequeux, J.-P. Korb, D. Petit, F. Barberon, B. Bresson, Phys. Rev. E 72 (2005) 041401.
[18] J.-P. Korb, Current Opinion in Colloid & Interface Science 14 (2009) 192.
[19] P.J. McDonald, J.-P. Korb, J. Mitchell, L. Monteilhet, Phys. Rev. E 72 (2005) 011409.
[20] L. Monteilhet, J.-P. Korb, J. Mitchell, P.J. McDonald, Phys. Rev. E 74 (2006) 061404.
[21] K.E. Washburn, P.T. Callaghan, Phys. Rev. Lett. 97 (2006) 17502.
[22] M. Fleury, J. Soualem, J. Coll. Interface Sci. 336 (2009) 250.
[23] J. Mitchell, M.D. Hürlimann, E.J. Fordham, J. Magn. Reson. 200 (2009) 198.
[24] M.D. Hürlimann, L. Venkataramanan, J. Magn. Reson. 157 (2002) 31.
[25] K.R. Brownstein, C.E. Tarr, Phys. Rev. A 19 (1979) 2446.
[26] J.J. Frippiat, M. Letellier, P. Levitz, M.J.M. Thomas, Trans. R. Soc. London Ser. A 311 (1984) 287.
[27] I. Solomon, Phys. Rev. 99 (1955) 559.
[28] N. Bloembergen, L.O. Morgan, J. Chem. Phys. 34 (1961) 842.
[29] A. Abragam, The Principles of Nuclear Magnetism, Clarendon, Oxford, 1961.
[30] P.L. Pratt, H.M. Jennings, Ann. Rev. Mater. Sci. 11 (1981) 123.
[31] J.-P. Korb, P.J. McDonald, L. Monteilhet, A.G. Kalinichev, R.J. Kirkpatrick, Cem. Concr. Res. 37 (2007) 348.
[32] E.R.T. Donaldson, P. Lorenz, SPE J. 9 (1969) 13.
[33] W.G. Anderson, J. Pet. Technol. 38 (1986) 1125.
[34] E. Amott, Trans. AIME 216 (1959) 156.
[35] A. Dixit, J. Buckley, S. McDougall, K. Sorbie, Transp. Porous Media 40 (2000) 27.
[36] W.J. Looyeesijn, Petrophys. 49 (2008) 130.
[37] M. Fleury, F. Deflandre, Magn. Reson. Imaging 21 (2003) 385.
[38] J. Chen, G.J. Hirasaki, M. Flaum, J. Pet. Sci. Eng. 52 (2006) 161.